Lux junior 2021

15. Internationales Forum für den lichttechnischen Nachwuchs
Ilmenau, 04. – 06. Juni 2021
DOI (proceedings): 10.22032/dbt.48427

DOI: 10.22032/dbt.49334

A model for predicting the visibility of intensity discontinuities in light patterns of vehicle headlamps

Katrin Schier [1], Mathias Niedling [1], Christoph Schierz [2]

[1]Institut für automobile Lichttechnik und Mechatronik (L-LAB), HELLA GmbH & Co. KGaA, Rixbecker Str. 75, 59552 Lippstadt

[2]TU Ilmenau, Fachgebiet Lichttechnik, Prof.-Schmidt Str. 26, 98693 Ilmenau

Abstract

High-resolution headlamps enable the generation of lane and symbol projections, offering additional information to the driver and other participants in traffic. While allowing the possibility of highlighting single pixels on the one hand, the light pattern without projections should give a smooth impression of the luminance distribution and should not show striking intensity differences between adjacent pixels. Which intensity differences lead to visible gaps in the light pattern is dependent on a set of numerous parameters.

A model for predicting the visibility of such intensity gaps for human observers is proposed here, a task which is directly linked to contrast detection. Hence the deployed model implements sequentially applied sub models based on the contrast sensitivity function (CSF).

In order to evaluate the model, it is tested with luminance distributions of a simulated pixelated light source as well as with a more complex scenario.

First evaluations of the model show promising results. For each tested scenario the model behaves as expected. The validity of the model will have to be verified by a study in a next step.

Index Terms: contrast sensitivity, computer vision, automotive lighting,

1 Introduction

Detecting objects or spots in a scene illuminated by headlamps is highly correlated with contrast detection. For road lighting the CIE report 19/2 [1] proposes to use the

visibility level which is based on psychophysical data measured by Blackwell [2] for predicting the detectability of a target in an illuminated environment. The visibility level is defined as the ratio of the contrast (between object and background) and the threshold contrast. While being a good measure for the detectability of objects in laboratory conditions, it is not applicable here, since a spot at an unknown position and not an object is to be detected.

Blakemore and Campbell [3] postulated that early visual processing mechanisms can be modeled by overlapping channels which are sensitive to different spatial frequencies. The authors introduced the reciprocal of the threshold contrast which is called the Contrast Sensitivity Function (CSF). The CSF is measured by showing images with sinusoidal gratings to the observer, since the frequency of these test patterns can be tuned very precisely.

The CSF is typically displayed in a diagram showing the contrast sensitivity over spatial frequency given in cycles per degree (cyc/deg). The sensitivity also changes with luminance. For lower luminances the sensitivity is reduced and the maximum sensitivity shifts to smaller frequencies (see Figure 2). As the human visual system is very complex and still not fully understood today, the CSF can only be a simplified model which will be limited to specific restrictions. Nevertheless, it has been successfully applied for multiple applications such as quality measurements for image compressing algorithms [4] or evaluation of vision of patients after eye surgery [5].

Joulan et al. [6] are the first to use the contrast sensitivity function in a context of automotive lighting for predicting the visibility of objects illuminated by a headlamp. They propose employing a multiscale spatial filter on luminance images which simulates the simple contrast perception of human vision. The filter consists of a weighted sum of Differential of Gaussians (DoG). The weights are adapted so the resulting filter corresponds to the CSF developed by Barten [7]. However, Barten stresses that his CSF model is only valid for photopic vision. Nighttime driving on the other hand delivers scenarios which are in the mesopic domain.

Here an approach splitting the effects of the optical system of the eye (optical CSF) and the neuronal processing of the retinal image (neuronal CSF) is used. The optical CSF includes effects like disability glare caused by stray light. The neuronal CSF simulates receptive fields of early stages of the human visual cortex. A third part inducing the threshold CSF concludes the model enabling the prediction of the visibility of a contrast. The chosen threshold CSF is valid for mesopic vision.

2 Model

As stated in section 1, predicting visual acuity is a highly complex topic. In order to develop a model with a reasonable number of parameters the following constraints are considered.

2.1 Constraints for the model design

- The model is only valid for foveal view. This includes angles of $-2° \leq \alpha \leq 2°$ [8]. This also means that stimuli do not have to be detected in the periphery before being focused.
- Contrast sensitivity is also dependent on the presentation time of the visual target [9]. Below 4 s [10] observation time the contrast sensitivity is reduced. Here only static scenarios are considered and the observers will be given more than 4s observation time for the stimuli. Hence the time dependence of the contrast sensitivity can be neglected.
- The model is designed for achromatic light patterns in a first step. If it's usability for the application of light pattern evaluation is confirmed, it is possible to expand its applicability to chromatic light patterns.
- The observation is always considered for binocular view of the stimulus.
- When observing contrasts with a specific frequency for the duration of about 1 minute contrast adaptation occurs [3], reducing the contrast sensitivity for the adapted frequency range. This effect is not regarded in the model. It is assumed the observer will only have about 30 s to view the stimuli.
- Special attention of the observer to specific regions leads to higher contrast sensitivities [11]. This effect is not regarded.

The model is designed for luminance images as input and consists of the following sub models, that are applied sequentially:

1. An optical CSF which simulates aberrations to the image by the optics of the human eye. Here the model of Watson is implemented [12].
2. A neuronal CSF which simulates the contrast detection mechanisms in the human retina. The CSF designed by Peli [13] is chosen for the application.
3. A CSF threshold function to which the results are compared. The CSF developed by Wuerger et al. [14] is selected as best applicable for the desired usage. It is designed for a large range of luminance levels and thus valid for mesopic vision.

A block diagram of the model is shown in Figure 1. Each sub model is explained in more detail in the following sections.

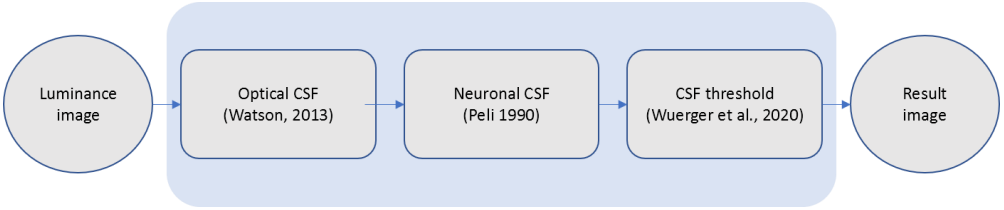

Figure 1: Setup of the proposed model

2.2 The optical contrast sensitivity function

The optical CSF describes the aberration of the image due to effects caused by the media of the eye. It can be used to calculate the resulting retinal image for a stimulus shown to a human observer [12]. Including the optical CSF in the model accounts for effects such as disability glare, which can have a large effect on the overall CSF.

The model implemented here was developed by Watson [12]. The pupil size, the age of the observer as well as the eye color influence the aberration and are thus considered as input parameters for the model.

Watson used the data of a large number of wavefront aberration measurements to develop the model. Zernike polynomials with the first 35 modes were implemented to match the measured aberrations [12]. From the results he calculated a mean radially symmetric real modulation transfer function and approximated a function which fits the data best. Additionally, the effect of scattered light is included, which reduces contrasts. Watson uses the formula found by Ijspeert et al. 1993 [15] to incorporate the influence of stray light.

As stated in [12] Watson's model concludes to:

$$CSF(r,d) = \left[1 + \left(\frac{r}{u_1(d)}\right)^2\right]^{-0.62} \cdot \sqrt{D(r,d,\lambda)} \cdot (1 - S(a,p)) \qquad (1)$$

with $r = \sqrt{u^2 + v^2}$, u is the horizontal spatial frequency and v the vertical spatial frequency. $u_1(d)$ is a polynomial fit which adapts the calculated CSF to different pupil diameters d. D considers the purely diffraction limited part of the CSF. It is calculated for white light with a center wavelength of λ = 555nm.

S considers the effect of scattered light. It is dependent on the pigmentation factor p and the age a of the observer, as well as the given reference age of 70 years. The equations for D, $u_1(d)$ and $S(a,p)$ can be found in Watson's publication ([12], equations (1), (4), (6))

Finally the pupil diameter is calculated as given in Watson et al. [16]. This model is an enhancement of the model designed by Stanley and Davies [17] and includes aging effects as well as a differentiation between binocular and monocular view. As stated in 2.1 the model proposed here is considered for binocular view. This results in the following equation for the calculation of the pupil diameter:

$$d_{\mathrm{SD}}(L,q) = 7.75 - 5.75\left(\frac{\left(\frac{L\cdot q}{846}\right)^{0.41}}{\left(\frac{L\cdot q}{846}\right)^{0.41}+2}\right) \tag{2}$$

The pupil's dynamic range is reduced with age. This is considered in the equation by adding an additional term:

$$d(L,q,a) = d_{SD}(L,q) + (a - a_{ref})\cdot(0.02132 - 0.009562\cdot d_{SD}(L,q)) \tag{3}$$

L is the mean luminance of the field of view (fov), q the area of the fov and a the age of the observer. The reference age $\mathrm{a_{ref}}$ is given to 28.58 years.

2.3 The neuronal modulation transfer function

The implemented modulation transfer function was developed by Peli [13]. It is originally applied to natural images (complex scenes) and enables the prediction if small details in the image are visible to the human observer.

2.3.1 Bandpass filters

The image is convoluted with different cosine log bandpass filters each having different center frequencies and a bandwidth of one octave. The filters in the spatial frequency domain are calculated to

$$G_{\mathrm{k}}(r) = 0.5\cdot(1+\cos(\pi\cdot\log_2 r - \pi\cdot k)) \tag{4}$$

Each filter has a center frequency of 2^k, with k being an integer value.

The filters designed here are very similar to Gabor filters, with the difference that the sum of the filters equals to unity [13]. Hubel and Wiesel [18] find that receptive fields have a close similarity to Gabor filter functions. The model is therefore a simplified approach for simulating early stages of visual processing, since it does not consider effects such as orientation selectivity as discovered by de Valois et al. [19].

The image is convoluted with each filter separately, delivering k results.

$$a_{\mathrm{k}}(x,y) = f(x,y) * g_{\mathrm{k}}(x,y) \tag{5}$$

With $f(x,y)$ being the image value at horizontal pixel position x and vertical pixel position y, $g_{\mathrm{k}}(x,y)$ being the k-th bandpass filter function in the spatial domain and $*$ representing the convolution operator. For the model proposed here the image is enlarged by half the filter size in each direction before filtering. The values at the borders of the image are repeated to avoid artificial edge creation. The resolution information of the image is not changed by this procedure and after filtering the image size is reduced to the original size again. This so-called padding avoids ringing artifacts created by the discrete Fourier transformation and is a very common procedure when multiplying filters in the frequency domain [20].

Since the model is designed for foveal vision the fov is limited to ± 2 degrees [8]. The area needed to display a full cycle at the smallest frequency should not exceed this region. Keeping to the design rule of Peli's model that the center frequency is given to 2^n the smallest frequency is chosen to $f_{c1}= 2^{-2}$ cyc/deg. The largest frequency applicable for the used setup is limited by the Nyquist frequency. Since the luminance images shown here have a resolution of ~ 75 pix/deg the maximum frequency that can be attained by Fourier transformation is given to 35 pix/deg. This results in a maximum center frequency of f_{c8} = 32 cyc/deg. The resulting frequencies explicitly chosen for the application of the here proposed model are thus given to: 0.5, 1, 2, 4, 8, 16 and 32 cyc/deg. In photopic lighting environments a healthy and young human observer is known to have a maximum resolution of 0.5' [21]. This corresponds to a resolution of 120 cyc/deg. In contrast to this the highest resolution of the model is set to only a fourth of this value. Figure 2 shows the contrast sensitivity for different luminances calculated by the model of Wuerger et al [14]. When comparing the maximum contrast sensitivity at 200 cd/m² to the contrast sensitivity of 0.2 cd/m² the maximum sensitivity drops to about one fourth of the value. Thus the chosen resolution could be sufficient for the model. To confirm if the model's resolution is adequate for the application a study with human observers is needed. If the results of the study should show that the resolution is not sufficient, the resolution of the systems can be increased. This is possible by using a lens with a larger focal length, thus increasing resolution at the cost of a decreasing fov. The center frequencies of the model will then need to be adapted to the Nyquist frequency for the new setup.

2.3.2 Contrast calculation

In order to account for neuronal adaptation processes Peli calculates the contrast for each channel by dividing the filtered images by an adaptation luminance value. The value is calculated by keeping only the frequencies in the image that are below the frequencies of the bandpass filter. The bandpass filtered image is then divided by the result:

$$c_{\mathrm{k}}(x,y) = \frac{a_{\mathrm{k}}(x,y)}{f(x,y) * l_{\mathrm{k}}(x,y)} \tag{6}$$

With $l_{\mathrm{k}}(x,y)$ being the lowpass filter in the spatial domain which is convoluted with the image.

2.3.3 Image reconstruction

The calculated contrast is compared to the threshold contrast for each pixel in each contrast image. If the contrast for the given center frequency of the bandpass is smaller than a given threshold the information in the bandpass filtered image at this pixel is discarded by setting the pixel to a value of zero.

$$a_{\mathrm{k}}(x,y) = \begin{cases} f(x,y) * g(x,y), & if\ c_{\mathrm{k}}(x,y) \geq c_{\mathrm{thresh}} \\ 0, & else \end{cases} \tag{7}$$

Peli uses the measured CSF of each single observer as threshold value [22]. After processing each bandpass filtered image this way the resulting image is reconstructed by a summation of all filtered and thresholded images, including the high- and lowpass residuals.

$$f_{\mathrm{rec}}(x,y) = l_0(x,y) + \sum_{\mathrm{k}=1}^{\mathrm{n}-1} a_{\mathrm{k}}(x,y) + h_{\mathrm{n}}(x,y) \tag{8}$$

With l_0 being the low pass residual and h_{n} being the high pass residual.

Even though Peli's results have a good correspondence to his study [23] this procedure is not directly applicable for the model proposed here. The goal is to develop a general approach, not one fit to individuals. For this reason a model predicting a mean CSF for healthy subjects is used to calculate the threshold value. The model is described in section 2.4.

2.4 The threshold function

The environment in which headlamps are typically used involves luminances below 3 cd/m², where the transition between the photopic and mesopic vision occurs [24]. It is therefore essential to choose a CSF which is valid for the mesopic vision region. The CSF used as threshold function chosen for this model was developed for adaptation luminances between 0.02 cd/m² and 7000 cd/m² [14]. It also incorporates a separable part which describes the chromatic CSF. This enables the possible expansion of the model in a later step without having to implement a different thresholding function.

Wuerger et al. develop the model as a continuous function dependent on the surrounding luminance and frequency, enabling the calculation for each average luminance or frequency found in the measured luminance distribution. They validate

the model with own measurement data as well as with a reasonable comparison to other data sets published. The authors propose an expansion of the model which includes the dependence of the CSF on the shown number of cycles. This expansion is not applied here, as the authors state that the amount of data to verify the expansion is not large enough. The resulting achromatic logarithmic CSF is thus calculated as follows:

$$S_{\log 10}(r, r_{\max}, b) = \log_{10}(S_{\max}) - \left(\frac{\log_{10}(r) - \log_{10}(r_{\max})}{0.5 \cdot 2^{b}}\right)^{2} \qquad (9)$$

With r being the radial frequency as used in the previous sections, $r_{\max}$ the frequency at which the CSF has its maximum value and $S_{\max}$ the maximum sensitivity at value $r_{\max}$. The calculations of the values for $r_{\max}$ and $S_{\max}$ can be found in Wuerger et al, [14], equations (16a,b).

The threshold contrast used for comparison can then be calculated by

$c_{\text{thresh}} = 10^{S_{\log 10}}$. The luminance L used for the calculation of the threshold is the mean luminance which is also used for the calculation of the contrast in (6).

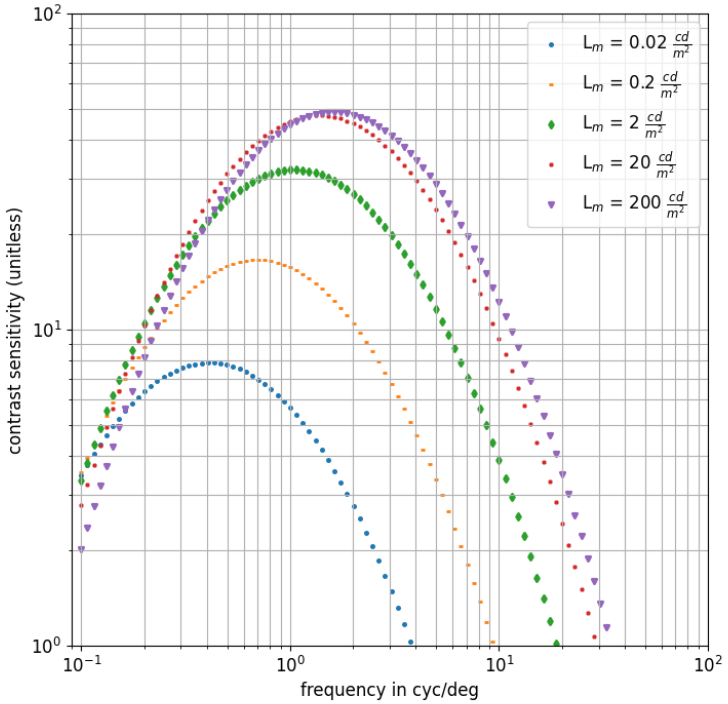

Figure 2: Contrast sensitivity function calculated with the model of Wuerger et al. [14] for different luminance levels.

3 Experimental

In order to get a first impression of the model's performance some test light patterns are created and the results are shown in the following section.

3.1 Setup

Generating a large variety of light patterns is essential for testing the model's applicability to headlamp light patterns. To enable testing a high-performance projector of the type Barco W30 Flex is used and calibrated geometrically and in terms of luminous intensity (as it receives 8-bit greyscale values as input data). The maximum luminous flux of the projector is given to 30,000 lumen. With an image size of 1920 x 1200 pixels and a corresponding field of view (fov) of ±15.03° in horizontal direction and ±10.05° in vertical direction, the resolution of the projector results to 0.017° vertically and 0.016° horizontally. The projector is located in the light tunnel of HELLA GmbH & Co. KGaA, which enables a stable testing environment independent of the daytime and weather conditions.

The model is tested with measured luminance images. They are generated with a luminance measurement camera of the type LMK5 Color, Techno Team, using a lens with a focal length of 16mm and a neutral density filter with a transmission of 7.93%.

The setup for the test is shown in Figure 3. The camera is placed 2m behind the projector and 1.2m above the road. The center of the projector lens is located 0.64 m above the road. Camera and projector are thus placed in positions that closely resemble headlamp and driver positions.

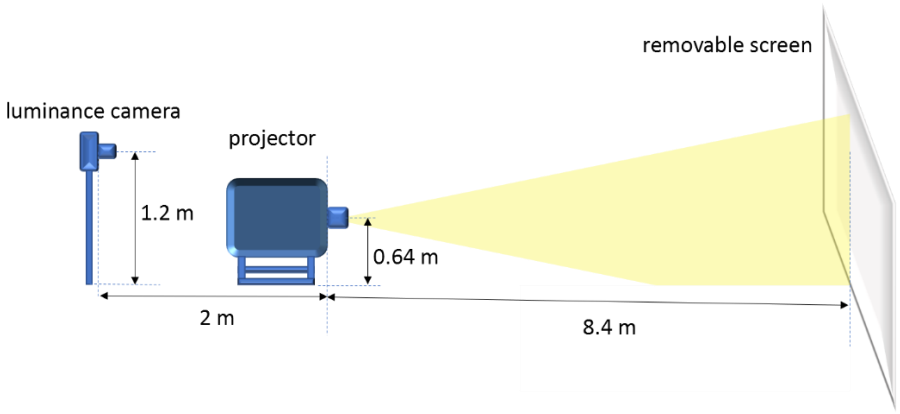

Figure 3: experimental setup in light channel

In order to translate the pixel positions into angular coordinates a point grid is used. The center of each point has a distance of 0.5° in vertical and in horizontal direction. With an image processing algorithm the center of the points in the luminance image is measured in pixel coordinates. In a next step the position is linked to the corresponding angle. With bilinear interpolation between the measured points each pixel in the image receives an angular coordinate in degree. After the projectors

angular positions are determined this way, the angular positions for the camera image can be calculated by knowing the distance to the projector's center.

The light pattern used for testing is generated by employing a simulated luminous intensity distribution of a headlamp module consisting of a high resolution pixelated light source. The simulation enables dimming and turning off single pixels completely.

Three different scenarios are examined:

1. A dark spot is created on an equally illuminated background, by turning off selected pixels. The size of the spot is then changed by turning off adjacent pixels. It is expected that the visibility improves with the size of the dark spot.
2. A bright spot is created on the same background and the size of the spot is changed in the same manner as before. The same principle behavior as for the dark spot is expected.
3. The last scenario shows a complex scene of a typical rural road with stationary road lighting. The effect of local adaptation on resolution is tested. It is expected that the visual acuity decreases in darker areas.

The first two scenarios are first projected to a white screen located at 8.4 m distance to the projector. Then the screen is removed and the same image is projected to the road. For the third scenario the light pattern is projected to the road only. The results are shown in the following subsection.

3.2 Results

The luminance images for the road and the screen are shown in Figure 4. For the analysis of the model's results a region of interest (roi) is chosen so only the surroundings in the proximity of the pixel is shown. The chosen roi is shown by the red boxes in Figure 4.

For the shown scenarios the observer age is set to 30 years, the observer's eye color is assumed to be brown.

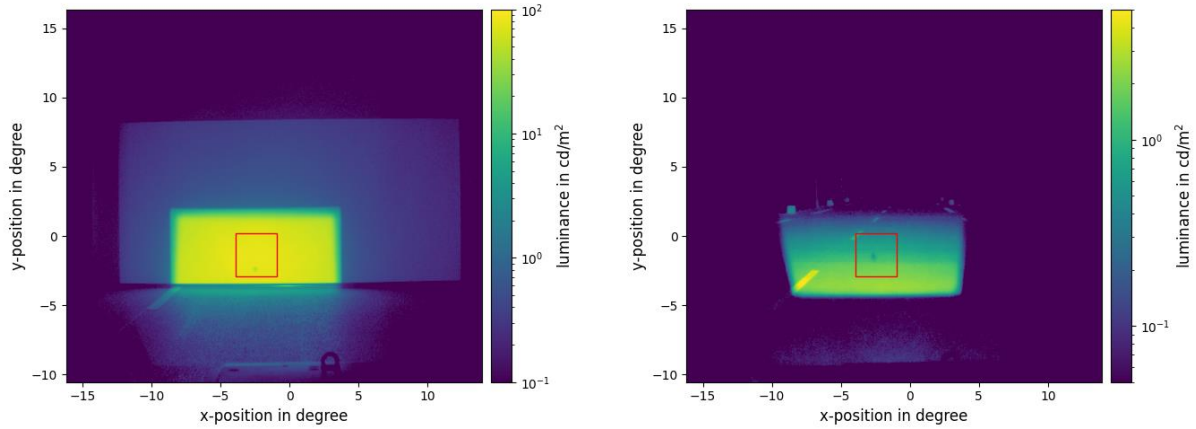

Figure 4: Luminance images for dark spot with a diameter of 0.4° projected to the screen (left) and to the road (right).

Scenario 1 – a dark spot changing in size:

Spot sizes with a diameter of 0.2°, 0.3° and 0.4° are created by dimming different amounts of adjacent pixels of the light source. The chosen simulation results in a surrounding luminous intensity of 16770 cd, and a luminous intensity of the spot of 11690 cd. In Figure 4 the results of the model are depicted exemplarily for the spot diameter of 0.4°.

The results of the image filtered with the bandpass filters of different center frequencies are shown in column 1. Bandpass filters with small center frequencies respond to spatially larger elements in the image and vice versa. Only the bandpass filters that have the highest response to the image (1, 2, and 4 cyc/deg) are shown in the figure.

The calculated contrasts and the threshold contrast can be seen in the second and third column of Figure 5 (screen projection) and Figure 6 (road projection). As contrast threshold changes with frequency, different thresholds are calculated for each center frequency. It is also very clearly visible that contrast thresholds change with luminance when comparing contrast thresholds on the road to the contrast threshold on the screen. The darker regions have a much higher threshold value.

The reconstructed image is shown in Figure 7, right image, bottom row. Stripe and circular shaped distortions are visible when looking at the image. These are due to the bandpass filtering (especially for smaller center frequencies) with thresholding and might lead to restrictions for the validity of the model when examining contrast just above the threshold value.

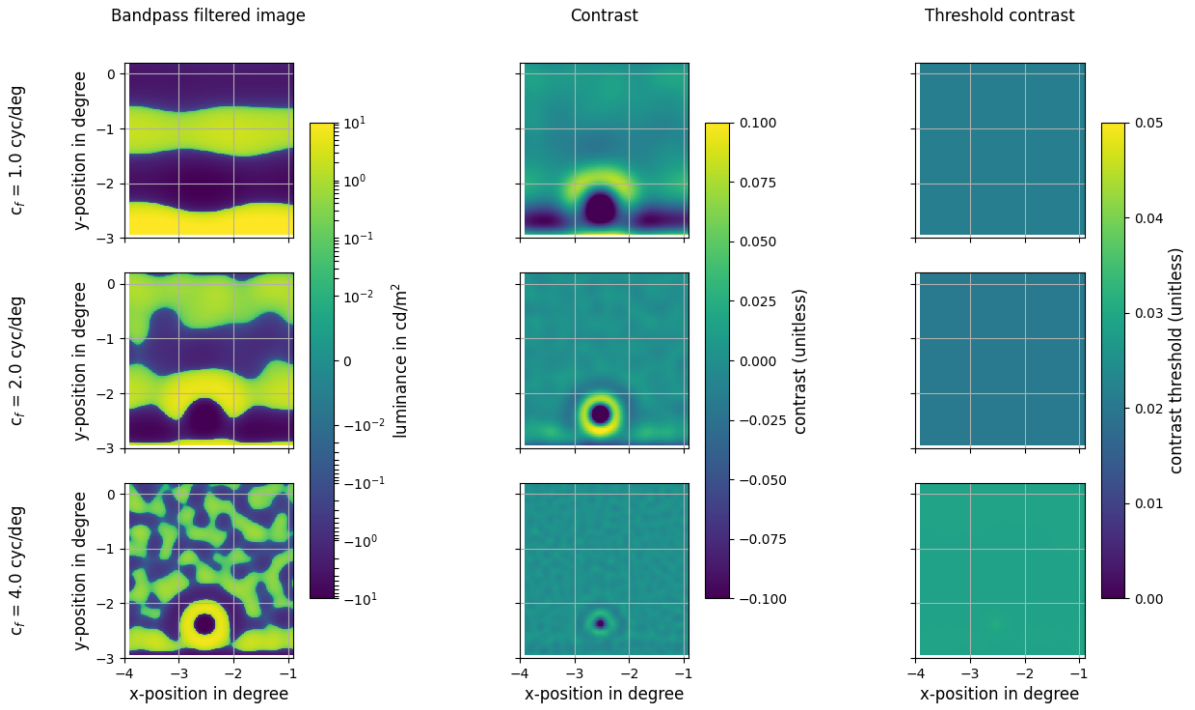

Figure 5: model results for dark spot with a diameter of 0.4°, projected to the screen shown for the roi marked by the red box shown in Figure 4.

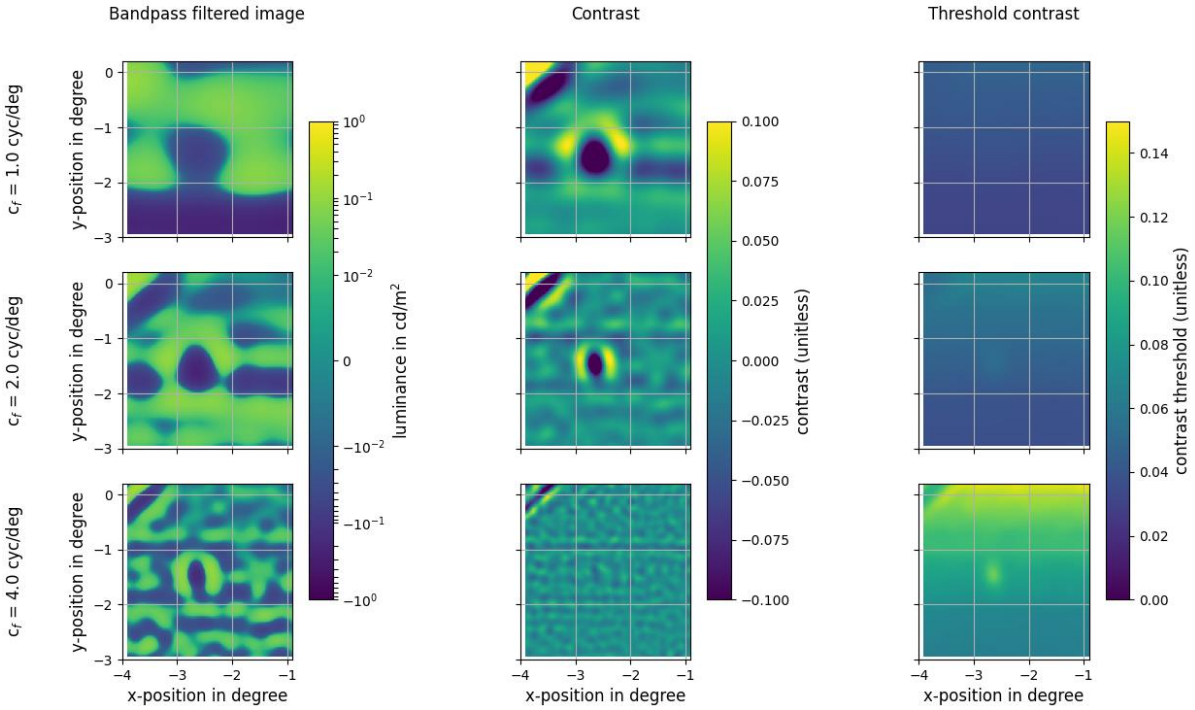

Figure 6: model results for dark spot with a diameter of 0.4°, projected to the road shown for the roi marked by the red box shown in Figure 4.

A comparison of the reconstructions for the different spot sizes are shown in Figure 7 for the projection to the screen. The smaller the spot size the larger the blurriness between the background and the screen. While a part of this effect is due to the reduced contrast by blurring of adjacent pixels, the model still shows the effect, as it is larger in the reconstruction than in the original.

Figure 8 shows the same experiment for the projection to the road. The model behaves exactly as expected. For smaller spot sizes the visibility is reduced until barely visible. This coincides very closely with the author's observations. These results deliver a first indication that the model is employable for the desired field of application.

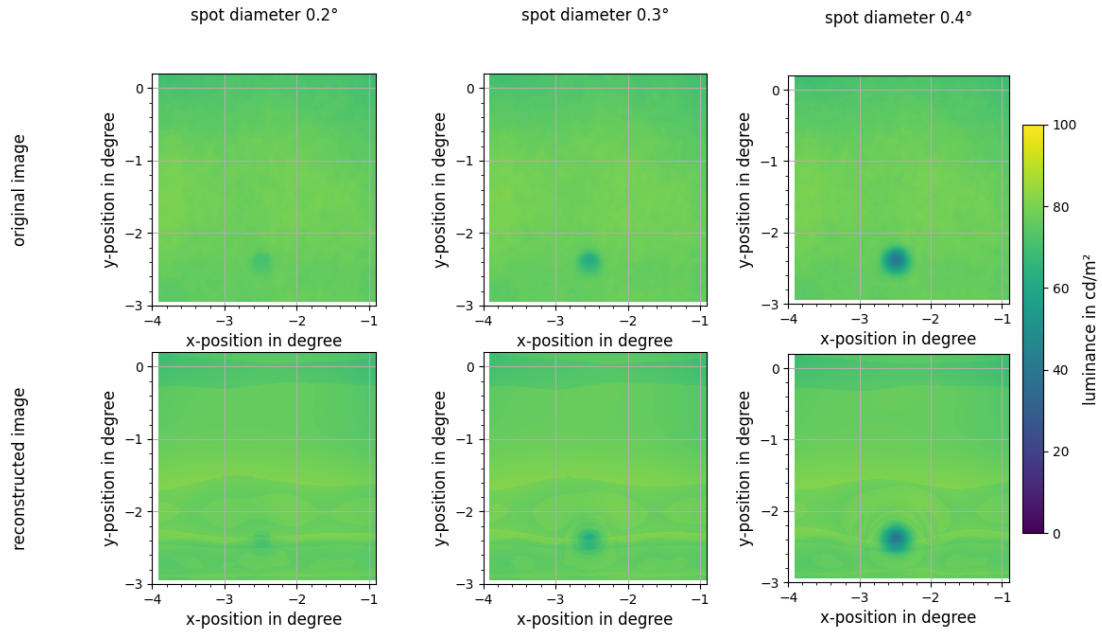

Figure 7: Original (top row) and reconstructed (bottom row) images of the dark spot with different diameters projected to the screen.

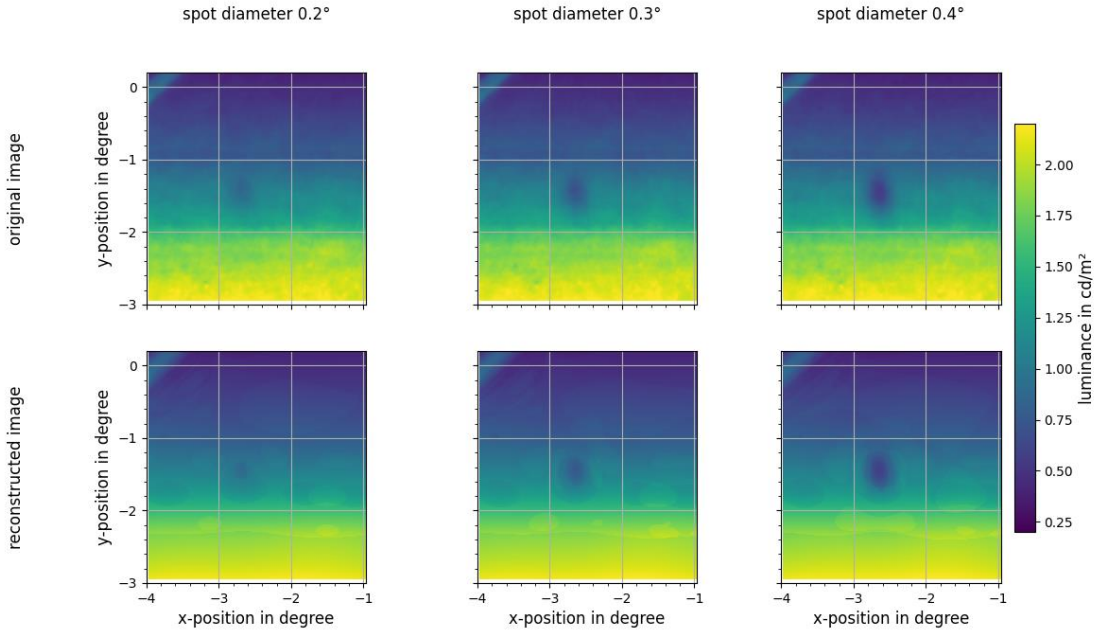

Figure 8: Original (top row) and reconstructed (bottom row) images of the dark spot with different diameters projected to the road.

Scenario 2 – a bright spot changing in size:

For the evaluation of detection quality for bright spots on an evenly illuminated background the same surrounding luminous intensity is used for the simulated light source as in scenario 1. The pixels creating the spots are set to a lower dimming level (higher intensity) than the surrounding. The luminous intensity for the bright spot is given to 21490 cd.

The resulting luminance distributions for the same roi as in scenario 1 as well as the reconstructed images are depicted in Figure 9 for the screen. In comparison to the original image the spot seems more blurred and less visible. This corresponds to the observed fact that the bright spot was harder to distinguish from the surrounding than the dark spot of the same size.

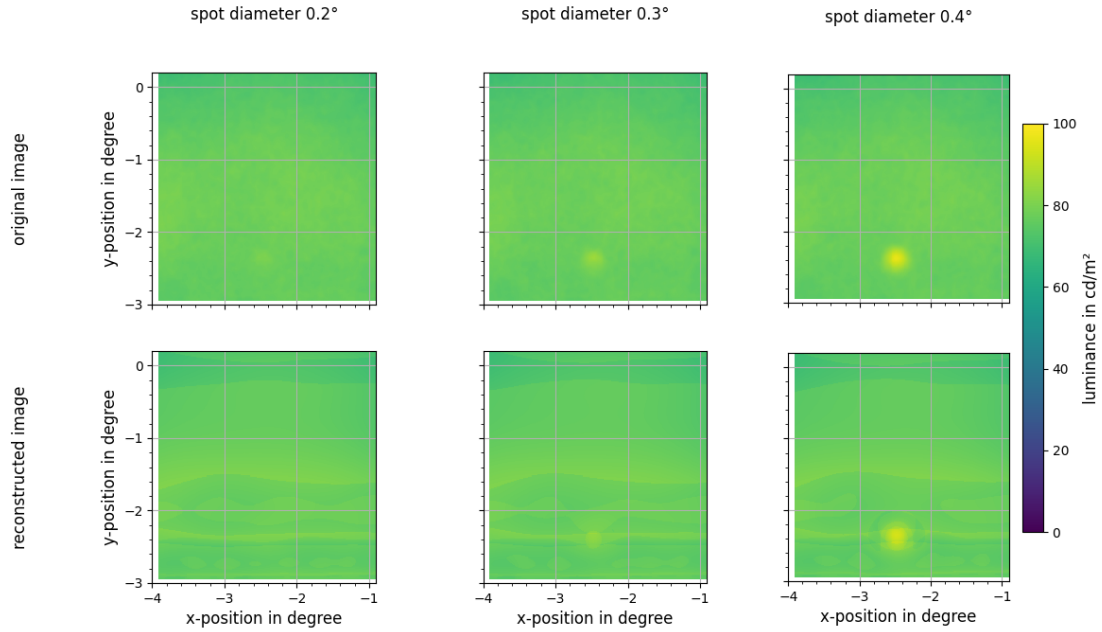

Figure 9: Original (top row) and reconstructed (bottom row) images of the bright spot with different diameters projected to the screen.

Scenario 3 – a complex scene:

The third scenario shows a more complex scene of a typical urban road at night (see Figure 10, left image). A low beam light distribution is illuminating the road in presence of stationary road lighting. Figure 11 shows the intermediate results of the neuronal CSF model.

The effects induced by the localized image evaluation of the model can be seen very clearly when comparing the contrast thresholds (column 3 in Figure 11) for the region of the trees (upper part of the image) to the contrast threshold in region of the road (lower part). The trees are not lit while the road is illuminated by the headlamps. The smaller luminance causes the CSF to shift to higher threshold values. For higher spatial frequencies this effect is increased. This leads to a more blurred image since the parts of the bandpass filtered images in which the contrast does not exceed the threshold value are not used for reconstruction. The dark trees in the reconstructed image (Figure 10, right image) are thus much more blurred than the traffic sign, which has a high luminance.

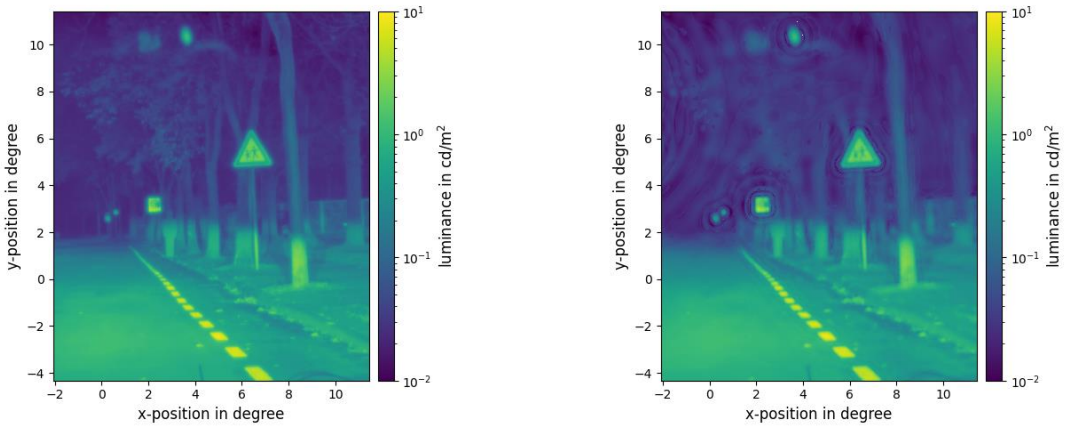

Figure 10: Luminance distribution of a complex scene (left) and the reconstructed image (right).

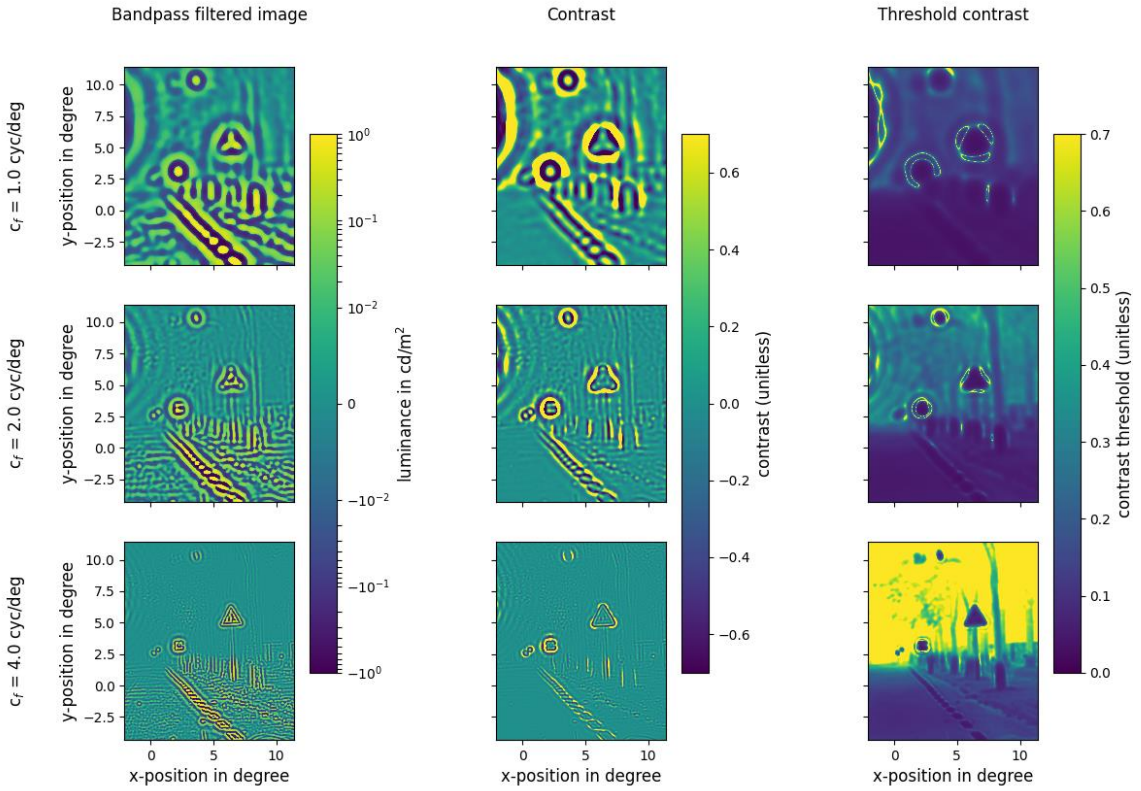

Figure 11: Intermediate results for the neuronal CSF with bandpass filtered images, calculated contrast, contrast threshold and reconstructed image.

This behavior of the model corresponds to the behavior of the human visual system. In dark environments small scale features cannot be distinguished anymore. The surrounding becomes more blurred and the acuity of the human visual system is reduced [14].

4 Summary and Conclusions

A model for predicting the visibility of dark or bright elements in a luminance distribution is proposed. It implements three sub models: A model for the influence of the optics of the eye (Watson [12]), a model for simulating the preliminary contrast detection of the human visual system (Peli [13]) and finally a model for detecting contrast thresholds for the mesopic region (Wuerger et al [14]). The proposed overall model is designed with some restrictions to its' validity: It is designed for static, foveal, binocular view with achromatic luminance distributions as input data and an observation time which allows neglecting temporal dependency as well as contrast adaptation effects.

The advantage of the model is the general applicability for a large variety of luminance distributions and surroundings, without need of parameter tuning. By using the three sub models effects such as disability glare and global as well as local luminance adaptation effects are regarded, when calculating the contrast.

The model's performance is examined using an equally lit background with a generated spot. For the positive as well as for the negative contrast the model's results correspond to the observed visibility. As the spot size is increased the visibility increases accordingly. The drawback of the model are distortions in the reconstructed image. These might lead to limitations on the model for predicting the visibility of contrast just above the threshold contrast.

In a last step the model is tested for a complex scene. For regions in the image with low luminances a much lower resolution of the reconstructed image is observed than for regions with higher luminances. This is again in accordance with the behavior of the human visual system. In dark surroundings the acuity of the visual system is reduced.

For all three scenarios the qualitative behavior of the model corresponds to the expected behavior. This is a very good indicator for the applicability of the model. The correspondence of the absolute values to the human visual system is currently unknown. To prove the validity of the model a careful study with human observers is indispensable.

5 References

[1] Commission Internationale de l'Eclairage, "An Analytic Model for Describing the Influence of Lighting Parameters upon Visual Performance", CIE publication 19/2, Vienna, 1981.

[2] H.R. Blackwell, "Contrast thresholds of the humane eye", Journal of the Optical Society of America, 1946.

[3] C. Blakemore, F. W. Campbell, “On the existence of neurones in the human visual system selectively sensitive to the orientation and size of retinal images”, Journal of Physiology, 203 (1), pp. 237-260, 1969

[4] M.J. Nadenau, J. Reichel, and M. Kunt, "Wavelet-based color image compression: exploiting the contrast sensitivity function.", IEEE Transactions on image processing, 12.1, pp: 58-70, 2003

[5] N. Yamane, K. Miyata, T. Samejima, T. Hiraoka, T. Kiuchi, F. Okamoto, Y. Hirohara, T. Mihashi, and T. Oshika, “Ocular higher-order aberrations and contrast sensitivity after conventional laser in situ keratomileusis”, Investigative Ophthalmology & Visual Science, 45(11), pp.3986-3990, 2004.

[6] K. Joulan, N. Hautiere, and N. Bremond, “Contrast sensitivity function for road visibility estimation on digital images”, Proc. 27th session of the Commission Internationale de l’Eclairage, 2011

[7] P. G. J. Barten, “Contrast sensitivity of the human eye and its effects on image quality”, SPIE press, 1999

[8] S. E. Palmer, Vision Science. Photons to Phenomenology, MIT Press, Cambridge, Massachusetts, 1999.

[9] F. L. Van Nes, J. J. Koenderink, H. Nas, and M. A. Bouman, "Spatiotemporal Modulation Transfer in the Human Eye," Journal of the Optical Society of America A, 57, 1082-1088, 1967

[10] B. Hauser, H. Ochsner, and E. Zrenner. "Der „Blendvisus”-Teil 1: Physiologische Grundlagen der Visusänderung bei steigender Testfeldleuchtdichte." *Klinische Monatsblätter für Augenheilkunde* (200.02), pp. 105-109, 1992

[11] N. V. K. Medathati, H. Neumann, G. S. Masson, and P. Kornprobst, ‘‘Bio-inspired computer vision: Towards a synergistic approach of artificial and biological vision”, Computer Vision and Image Understanding, vol. 150, pp. 1–30, 2016.

[12] A.B. Watson, "A formula for the mean human optical modulation transfer function as a function of pupil size." Journal of Vision, 13.6, 18-18, 2013

[13] E. Peli, “Contrast in complex images”. Journal of the Optical Society of America A, 7, 10, 2032-2040, 1990

[14] S. Wuerger, M. Ashraf, M. Kim, J. Martinovic, M. Pérez-Ortiz, and R. K. Mantiuk, “Spatio-chromatic contrast sensitivity under mesopic and photopic light levels”, Journal of Vision, 20(4), 2020

[15] J. K. Ijspeert, T. J. T. P. Van Den Berg, and H. Spekreijse, "An improved mathematical description of the foveal visual point spread function with parameters for age, pupil size and pigmentation." Vision research 33(1) pp: 15-20, 1993.

[16] A.B. Watson, and J. I. Yellott, "A unified formula for light-adapted pupil size.", Journal of vision, 12.10, 12-12, 2012

[17] P. A. Stanley, and A.K. Davies, “The effect of field of view size on steady-state pupil diameter.”, Ophthalmic & Physiological Optics, 15(6), pp. 601–603, 1995

[18] D.H. Hubel, and T. Wiesel, “Receptive fields, binocular interaction, and functional architecture in the cat’s visual cortex”, Journal of Physiology, London, 160:106–154, 1962

[19] R. L. de Valois, D. G. Albrecht, and L. G. Thorell, “Spatial frequency selectivity of cells in macaque visual cortex”, Vision Research, 22(5), pp.545–559,1982

[20] A. Distante, and C. Distante, Handbook of Image Processing and Computer Vision. Volume 1: From Energy to Image, p. 438, Springer International Publishing, 2020.

[21] J.A. Ferwerda, "Elements of early vision for computer graphics.", IEEE computer graphics and applications 21.5 pp: 22-33, 2001

[22] E. Peli, "Test of a model of foveal vision by using simulations.", Journal of the Optical Society of America A, 13.6, 1131-1138, 1996

[23] E. Peli, "Contrast sensitivity function and image discrimination," Journal of the Optical Society of America A, 18, 283-293, 2001

[24] B. Wördenweber, P. Boyce, D.D. Hoffmann and J. Wallaschek, “Automotive lighting and human vision”, Vol. 1., Springer-Verlag, Berlin Heidelberg, 2007.